Annual cycle of turbulent dissipation estimated from Seagliders

Dafydd Gwyn Evans[1], Natasha Sarah Lucas[2], Victoria Hemsley[3], Eleanor

Frajka-Williams[1], Alberto C. Naveira Garabato[1], Adrian Martin[4], Stuart C.

Painter[4], Mark Inall[5] and Matthew Palmer[6]

———

Dafydd Gwyn Evans, dafydd.evans@noc.soton.ac.uk

[1]Ocean and Earth Science, University of

Southampton, National Oceanography

Centre Southampton, European Way,

Southampton, UK.

[2]School of Ocean Sciences, Bangor

University, Askew St, Menai Bridge,

Anglesey, UK

[3]Queen Mary University London

[4]National Oceanography Centre,

Southampton, UK.

[5]Scottish Association for Marine Science

The rate of dissipation of turbulent kinetic energy is estimated using Seaglider observations of vertical water velocity in the mid-latitude North Atlantic. This estimate is based on the large-eddy method (LEM), allowing the use of measurements of turbulent energy at large scales $O(1\text{--}10 \text{ m})$ to diagnose the rate of energy dissipated through viscous processes at scales $O(1 \text{ mm})$. The Seaglider data considered here was obtained in a region of high stratification ($1 \times 10^{-4} < N < 1 \times 10^{-2} \text{ s}^{-1}$), where previous implementations of this method fail. The LEM is generalized to high-stratification by high-pass filtering vertical velocity with a cut-off dependent on the local buoyancy frequency, producing a year-long time series of dissipation rate spanning the uppermost 1000 m with sub-daily resolution. This is compared to the dissipation rate estimated from a moored 600 kHz Acoustic Doppler Current Profiler. The variability of the Seaglider-based dissipation correlates with one-dimensional scalings of wind and buoyancy driven mixed-layer turbulence.

Keypoints:

• Generalized method of estimating dissipation rate from Seagliders filtered by stratification

---
[6]National Oceanography Centre,

Liverpool

- Annual cycle of turbulent dissipation in the top 1000 m in the North Atlantic

- One-dimensional scaling for wind and buoyancy derived turbulence explain annual cycle of dissipation

1. Introduction

The exchange of heat, momentum and carbon dioxide between the atmosphere and ocean is governed by the turbulent processes that occur within the mixed layer. These turbulent processes are driven by interactions between wind, waves, surface buoyancy loss and horizontal buoyancy gradients in the upper ocean. Classical one-dimensional representations of mixed layer turbulence rely on simple scalings of surface forcing due to surface buoyancy loss and wind stress [*Pollard et al.*, 1972; *Tennekes and Lumley*, 1972; *Shay and Gregg*, 1984; *Gargett*, 1989; *Large et al.*, 1994; *Thorpe*, 2005]. Recent advances in the theory of submesoscale processes suggest an important role in the generation of turbulence for instabilities associated with strong horizontal buoyancy gradients and for Langmuir turbulence from the interaction between the mean flow and Stokes drift [*Hoskins*, 1982; *Belcher et al.*, 2012; *Thomas et al.*, 2013; *Buckingham et al.*, 2016; *Thompson et al.*, 2016; *Li et al.*, 2017]. The relevance of one-dimensional representations of ocean turbulence compared to those associated with three-dimensional submesoscale motions remains an important question, particularly for simulating accurate mixed layer depths in ocean climate models [*Belcher et al.*, 2012].

Oceanic turbulence acts to enhance the mixing of momentum, heat, salt and carbon compared to the rates associated with molecular diffusion [*Tennekes and Lumley*, 1972]. The dissipation of turbulent kinetic energy at rate ϵ and the associated energy lost through viscous processes therefore acts as an important sink in the global ocean energy budget, balancing the energy input to the ocean by wind and the sun [*Wunsch and Ferrari*, 2004; *Ferrari and Wunsch*, 2008]. Turbulence exists at scales of $O(10^{-3}\text{-}10^{1})$m, and is therefore

not resolved in a wide spectrum of numerical models. It is instead parameterized as a scalar 'eddy diffusivity', the suitability of which depends on how well turbulent processes are understood [e.g. *Griffies et al.*, 2005]. Further, the mixing associated with oceanic turbulence also impacts the rates of biological production and associated carbon export by affecting the vertical distribution of nutrients and plankton within the nutrient-limited euphotic zone [*Sarmiento and Gruber*, 2006]. Yet estimates of the magnitude, variability and spatial distribution of dissipation both within and below the mixed layer remain scarce.

Estimates of dissipation are traditionally limited to point estimates from vertical microstructure profilers [*Sheen et al.*, 2013]. These provide very high resolution data in the vertical, but have limited spatial and temporal coverage. Other direct estimates involve tethered/bottom mounted acoustic doppler current profilers (ADCP), which give very high temporal coverage during the course of a mooring deployment, but provide limited spatial or vertical information [*Lucas et al.*, 2014; *Polzin et al.*, 2014]. Indirect estimates of the enhanced mixing associated with turbulence (i.e. those that do not physically measure turbulent overturns) are derived from tracer release experiments or inverse methods. These provide a net rate of mixing based on the time- and space-integrated evolution of a tracer [*Watson et al.*, 2013], or the balance assumed to maintain a steady-state density field [*Zika et al.*, 2010]. Each method has some limitations, particularly in resolving the spatio-temporal variability of mixing that is critical to determine the underpinning physical processes. Recent developments utilizing the vertical water velocity estimated from Seagliders look to fill this gap by increasing the temporal and spatial coverage of direct

dissipation estimates, given the long endurance (4-6 months) of autonomous Seaglider missions [*Beaird et al.*, 2012].

In this article, we present a year-long time series of the estimated dissipation rate from the surface to 1000 m, and assess the processes that drive changes in the depth of the actively mixing layer in the upper ocean. This reveals that upper-ocean dissipation can be largely explained by simple classical scalings for the turbulence generated by the buoyancy fluxes and wind stress acting on the sea surface. Previous estimates of turbulent dissipation from Seagliders use the large-eddy method, in which the kinetic energy of the largest turbulent eddies is assumed to feed turbulent dissipation at the smallest scales. A key step in this method is to separate internal wave motions from turbulent eddies. *Beaird et al.* [2012] found that a 30 m high-pass filter was appropriate to separate waves from overturns in the subpolar North Atlantic. Here, we generalize the method by developing a filter with a cut-off dependent on the local buoyancy frequency, which sets the high-frequency limit of the internal wave band [*D'Asaro and Lien*, 2000].

In the following section, we introduce the Seaglider data set and detail the methodology used to estimate the rate of dissipation. We also outline a set of classical scalings for upper-ocean dissipation. In section 3, we compare the Seaglider-based estimate of dissipation rate to an independent estimate from a moored Acoustic Doppler Current Profiler (ADCP), and assess the agreement between the Seaglider-derived dissipation and the classical scalings for upper-ocean dissipation. In the final section, we summarize the results of this study.

2. Data and Methods

Temperature, salinity and pressure profiles from Seagliders in the northeast Atlantic were used to estimate the dissipation of turbulent kinetic energy by applying the large-eddy method (LEM). Seagliders are autonomous underwater vehicles that control their position within the water column by pumping oil in and out of an external bladder, thus varying their density by adjusting their volume [*Eriksen et al.*, 2001]. Seaglider missions are typically designed to profile vertically (from the surface to 1000 m) in a saw-tooth fashion, transmitting the data collected by onboard conductivity, temperature and pressure sensors via satellite at the sea surface. The Seaglider data used in this analysis were collected as part of the Ocean Surface Mixing, Ocean Submesoscale Interaction Study (OSMOSIS; NERC grant NE/I019999/1). The time-series of Seaglider data is composed of three separate missions that are described in detail within *Damerell et al.* [2016] and *Thompson et al.* [2016]. The complete time-series extends from September 2012 to September 2013, and the three missions combine to give a total of 4099 profiles. The Seagliders sampled between 48.6°N, 48.8°N, 16.3°W and 16.1°W (Figure S6a; also see figures 1,3 and 4 in *Thompson et al.* [2016]). The nominal sampling interval at depths less than 300 m is approximately 5 seconds, but can be as high as 8-10 seconds depending on the control operations the glider performs. Below 300 m the nominal sampling frequency is ∼10 seconds, but may also be longer. The irregularity of the sampling interval and the change at 300 m can add noise to the energy spectra of vertical velocity.

Vertical water velocity is calculated by comparing the vertical profiling speed of the Seaglider to an idealized model of the Seaglider flight determined from the vertical density profile and the lift/drag/buoyancy characteristics of the Seaglider [*Frajka-Williams et al.*,

2011]. Following from *Frajka-Williams et al.* [2011] we remove data from the 25 second period following a controlled change in the glider roll or pitch. Further, we discard data within 40 m of the profile apogees. During controlled glider maneuvers the assumption of steady flight that is critical to the glider flight model does not hold.

The scale of turbulent dissipation in the ocean is on the order of millimeters. Gliders cannot measure at this scale, so a dissipation rate estimate from glider vertical velocity must rely on a scaling of the turbulent kinetic energy equation. The scaling used here is the LEM applied to Seaglider data [*Beaird et al.*, 2012]. This scaling is based on the assumption of a steady cascade of energy from the largest scales of turbulent motions to the viscous scales at which energy is dissipated [*Taylor*, 1935; *Moum*, 1996]. In steady state and assuming no leakage of energy, dissipation at viscous scales can therefore be determined from the kinetic energy velocity scale (q') in the largest turbulent eddies of $O(1 - 10)$ m and their overturning time scale yielding $\epsilon \sim (q')^3/l$ [*Gargett*, 1999]. The scales of the largest turbulent eddies are resolved by glider sampling.

The choice of the turbulence length scale l is an important one, and is ideally represented by the Thorpe length scale if high-resolution vertical density profiles are available [*Thorpe*, 1977]. Alternative estimates of l have been extensively discussed in previous studies [e.g. *Gargett*, 1999]. The Ozmidov length scale, $L_{Oz} = \epsilon^{1/2} N^{-3/2}$, is one such scale, and is the largest turbulent eddy that is unaffected by stratification [*Dillon*, 1982]. Observations suggest a linear relationship between the Thrope length scale and the Ozmidov length scale, both within the weakly stratified mixed layer and strongly stratified pycnocline [*Dillon*, 1982; *Wesson and Gregg*, 2012; *Ferron et al.*, 1998].

Beaird et al. [2012] applied the LEM in estimating dissipation from glider vertical velocity using observations from the weakly stratified subpolar North Atlantic. Using the Ozmidov length scale for l, they present an estimate of dissipation in terms of a velocity scale q' and the buoyancy frequency N as

$$e = c_\epsilon N(q')^2, \tag{1}$$

where c_ϵ is a constant of proportionality that acts to scale the estimate of the rate of dissipation (e) relative to a direct measurement of this variable. To calculate N, we adiabatically redistribute (sort) fluid parcels according to the methodology outlined in *Bray and Fofonoff* [1981]. This represents the background stratification acting to restore a turbulent overturn. When computed using a sorted N, the Ozmidov length scale matches the Thorpe length scale even in the mixed layer [*Dillon*, 1982]. Within this dataset, when computed using the unsorted density profile, $\sim 28\%$ of mixed layer N data points are negative. The velocity scale q' is defined as the rms of the vertical velocity.

To estimate the rate of dissipation from the vertical water velocity, *Beaird et al.* [2012] first filter vertical velocity to remove low-frequency internal wave variability using a high-pass filter with a fixed 30 m cut-off. When applied here in more strongly stratified waters, this cut-off wavelength fails to remove internal wave variability as the vertical stratification is stronger and more variable. Freely propagating internal waves have frequencies (ω) in the range $f < \omega < N$ where f is the Coriolis parameter [*D'Asaro and Lien*, 2000]. Here, we use an alternative approach to define q' by using an adaptive high-pass fourth-order Butterworth filter set to the value of the vertical stratification N. When N is large, this filter should isolate turbulent processes within the inertial subrange. When N is very low,

within the surface mixed layer for example, this filtering acts to remove the mean and any trend with respect to depth from the vertical velocity. Note that in the case of an inadequately tuned flight or flight model, spurious vertical velocity signals may appear as a mean or trend with depth [*Frajka-Williams et al.*, 2011] Dissipation is calculated in 20 m vertical bins from the surface to 900 m. To validate the LEM method, we use a time-series of dissipation estimated from a moored 600 kHz ADCP (deployed as part of the OSMOSIS field campaign) using the structure function method outlined in *Lucas et al.* [2014] and within the Supplementary Information [*Lhermitte*, 1969; *Sauvageot*, 1992; *Zedel et al.*, 1996; *Rippeth et al.*, 2003; *Wiles et al.*, 2006; *Lorke*, 2007; *Lorke et al.*, 2008; *Mohrholz et al.*, 2008; *Thomson et al.*, 2010; *Liu et al.*, 2011; *RDInstruments*, 2011; *Rudnick and Cole*, 2011; *Simpson et al.*, 2011; *Thomson et al.*, 2012; *Talke et al.*, 2013; *McCaffrey et al.*, 2015; *Rumyantseva et al.*, 2015; *Simpson et al.*, 2015; *McMillan et al.*, 2016; *Horwitz and Hay*, 2017; *Guerra and Thomson*, 2017; *McMillan and Hay*, 2017; *Scannell et al.*, 2017]. The ADCP is mounted at ∼50 m on the central mooring (48.7°N, 16.2°W) of the OSMOSIS mooring array [*Buckingham et al.*, 2016; *Damerell et al.*, 2016], providing a full annual time series of the rate of dissipation coinciding with the glider deployments.

As an alternative to the Ozmidov length scale, we computed e using Thorpe length scales. This approach underestimated the dissipation rate below the mixed layer, but matched the magnitude of the ADCP-based dissipation rate when the mixed layer deepened to below the depth of the ADCP. The low vertical sampling resolution (∼0.8–1.5 m) of the Seaglider-based density profile likely results in an overestimate of Thorpe length scales, and an underestimate of e when N is high. *Beaird et al.* [2012] describe similar

issues when using the Thorpe length scale for l when applying the LEM. Consequently, we use the Ozmidov length scale throughout.

There are some general limitations to this approach that should be noted. As mentioned above, the glider flight model assumes steady flight. Controlled changes to the glider roll and pitch can be limited by increasing the interval at which the glider activates the guidance and control systems. This is not practical near the surface and at apogee, which is why we remove data within 40 m of the profile apogee. Consequently, our dissipation rate estimate will miss some of the surface mixed layer that is shallower than 40 m. We indicate periods within the glider time series when excessive roll maneuvers affect the dissipation rate estimate. Further, to determine c_ϵ, comparison to an existing estimate of dissipation rate is required, which should cover a representative range of dissipations. Here, we utilize a time series of dissipation rate estimated from the moored 600 kHz ADCP, as this has been evaluated against direct estimates of dissipation rate from microstructure profilers. The value of c_ϵ and the magnitude of e is therefore dependent on any uncertainty in the ADCP-based dissipation rate.

Further considerations were required for the Seaglider data specific to this study due to the irregular sampling interval of the glider's CTD, resulting in a step change in the estimated dissipation rate at 300 m. As discussed in the Supporting Information removing this step change required filtering with a band pass filter with a low-frequency cut-off at N and a high-frequency cut-off at 1/60 s [*Lomb*, 1976].

We compare the updated glider estimate of dissipation rate to the dissipation rate expected from surface air–sea heat fluxes and wind-stress using daily fields for shortwave

radiation, longwave radiation, latent heat flux, sensible heat flux and 10 m winds from the ERA-Interim reanalysis product [*Dee et al.*, 2011]. Using fields with a horizontal resolution of 0.75°, data were selected from the grid cell at 48.75°N and 16.5°W to coincide with the glider data. Wind stress is calculated based on the approach of *Large and Pond* [1981] and *Trenberth et al.* [1990] at low wind speeds (Figure S6b and S6c; our conclusions are not affected by the choice of wind-stress algorithm). When the Earth's rotation is ignored, the simplest estimates of turbulence in the mixed layer are governed by buoyant convection and wind-driven surface shear stress [*Shay and Gregg*, 1984, 1986; *Gargett*, 1989]. Convection in the mixed layer is driven by a surface buoyancy flux B_0, given by

$$B_0 = -g\rho^{-1}[\alpha c_p^{-1}(Q_{SW} + Q_{LW} + Q_{LH} + Q_{SH}) + \beta Q_{LH}L^{-1}S], \qquad (2)$$

where g is the acceleration due to gravity, ρ the mixed layer density, c_p the specific heat capacity of seawater ($\sim 4 \times 10^3 \, \mathrm{J\,kg^{-1}K^{-1}}$), L the latent heat of evaporation ($\sim 2.5 \times 10^6 \, \mathrm{J\,kg^{-1}}$) and S the mixed layer salinity [*Shay and Gregg*, 1986]. The coefficients α and β represent the thermal expansion and haline contraction of seawater, while Q_{SW}, Q_{LW}, Q_{LH} and Q_{SH} are heat fluxes due to incoming short wave radiation, outgoing longwave radiation, the latent heat of evaporation and sensible heat flux, respectively. Assuming a linear decrease through the mixed layer [*Gargett*, 1989], B_0 gives an estimate of the dissipation of turbulent kinetic energy by convection (ϵ_Q) as

$$\epsilon_Q = \frac{1}{2}B_0H \qquad (3)$$

where H is the mixed layer depth, determined here as the depth at which the density exceeds the density at 10 m by 0.03 $\mathrm{kg\,m^{-3}}$.

An estimate of the rate of dissipation associated with wind-driven turbulence (ϵ_τ) can be made by using the wall-layer scaling [e.g. *Tennekes and Lumley*, 1972; *Thorpe*, 2005] for the vertical extent of shear-driven eddies

$$\epsilon_\tau = \int_{-H}^{0} \frac{u_*^3}{\kappa z} dz, \tag{4}$$

where $\kappa = 0.4$ is the von Karman constant and z depth. The scale u_* for vertical turbulent velocities is determined from the surface wind stress τ as

$$u_* = \sqrt{\frac{\tau}{\rho}}. \tag{5}$$

Dissipation due to breaking surface waves is likely to be one order of magnitude greater than ϵ_Q and ϵ_τ. However, as discussed above, we do not use the glider dissipation at depths less than 40 m. These depths are beyond the influence of breaking surface waves and will not capture a substantial portion of the wind-driven turbulence. [*Gargett*, 1989; *Thorpe*, 2005].

3. Results

In order to estimate the rate of dissipation using the methodology described in section 2, the value of c_ϵ must be determined by comparison with a simultaneous estimate of the dissipation. Here, we compare the glider estimate of dissipation rate to a time series of dissipation calculated from the moored 600 kHz ADCP (Figure 1). The nearest depth bin to the measured ADCP depth is selected from the Seaglider estimate of dissipation. A linear least squares fit between the three glider deployments and the ADCP dissipation rate estimate yields $c_\epsilon = 1.96 \pm 0.2$. The full time series are displayed in Figure 1a, with confidence intervals computed at the 90% level using a Monte Carlo approach. We

perform 5000 simulations for which we randomly sample 90% of the data points with replacement used to determine the displayed 4-day mean. The glider and ADCP estimates of dissipation rate generally agree within the confidence interval of the glider estimate, except during periods of excessive glider roll maneuvers, indicated by the gray shading (also see Figure S7 in the Supporting Information).

During the first two glider deployments, from September 2012 to April 2013, when stratification at the ADCP depth was weakening in the transition to winter, the glider and ADCP estimates show dissipation levels of 10^{-7} W kg^{-1} to 10^{-6} W kg^{-1}, with good agreement illustrated by a correlation coefficient between the filtered time-series of r=0.81 (Figure 1a). From May onwards, during the third glider deployment, there are sporadic periods of disagreement. In May and June, agreement was poor when the glider is a distance of >10 km from the ADCP mooring. Conversely, in January when the distance between the glider and ADCP mooring increases beyond 10 km, the agreement between dissipation estimates remains good. This may suggest that turbulence levels are coherent over a lateral extent of $O(10)$ km in the winter, and less so in May / June. Agreement between the glider and ADCP was also poor in August to September 2013 when excessive glider rolling reduced reliability (gray shading; Figure 1a). The glider and ADCP dissipation averaged into bins of buoyancy frequency N also suggest a good agreement between ADCP and glider estimates (Figure 1c). At low N, the glider estimate appears to underestimate the rate of dissipation, associated with periods when the glider dissipation falls short of peaks in ADCP dissipation during the winter. The agreement is also less good at some high values of N, but the glider data is affected by excessive roll maneuvers.

A comparison between the method used here to estimate dissipation rate from glider measurements and the method outlined in *Beaird et al.* [2012] is also made in Figure 1a and Figure 1c. This indicates that the generalized method described here better estimates the rate of dissipation during summer and autumn / fall, when the *Beaird et al.* [2012] method overestimates dissipation. Stratification is highest during these periods, and a filter that passes variations with a wavelength less than 30 m seems to be insufficient to remove internal wave-related signals. When averaged in to bins of N, the dissipation rate estimated using the *Beaird et al.* [2012] method underestimates the dissipation rate at low N and overestimates the dissipation at high N.

Using the scale factor (c_ϵ) derived from the glider / ADCP comparison, we can then estimate the full annual cycle of dissipation rate from the surface to 1000 m at 48.7°N, 16.2°W (Figure 2a). In Figure 2 we include data shallower than 40 m, except during spring when data quality was poor due to excessive roll maneuvers (see Figure 1 and Figure S7). No data shallower than 40 m was used for comparison with ADCP dissipation rate. Through the fall, coinciding with pulses in the dissipation rates of $O(10^{-6})\,\mathrm{W\,kg^{-1}}$, stratification breaks down as the mixed layer deepens. The mixed layer remains at a depth of approximately 200 m during January–April, reaching a maximum of ∼400 m in February. Through the spring and early summer of 2013, the mixed layer shoals rapidly as stratification increases. This shoaling is interspersed with daily to weekly changes in mixed layer depth that correspond to sporadic periods of elevated dissipation. Below the mixed layer, the vertical profile of dissipation reaches a minimum of $O(10^{-9})\,\mathrm{W\,kg^{-1}}$

between 200 m and 600 m where stratification is weakest. Below 600 m the estimated dissipation is higher where stratification is elevated.

Previous analyses in this region have focussed on the importance of submesoscale instabilities in driving elevated turbulence within the mixed layer [*Thompson et al.*, 2016]. Here, to understand the processes that govern dissipation within the upper ocean, we compare simple scalings for turbulence due to surface buoyancy loss and wind stress to the mixed layer-integrated glider dissipation neglecting dissipation shallower than 40 m (Figure 3). Below 40 m, we do not expect our glider estimate to be influenced by surface waves, which influence the profile of ϵ within a few significant wave heights of the surface [*D'Asaro*, 2014]. In general, wind-driven mixed layer dissipation is higher than dissipation by buoyant convection, more closely matching the magnitude of the glider dissipation rate (Figure 3a, c and d). The relative contributions of wind stress and buoyant convection do however vary throughout the year. For example, from September through November, as the mixed layer deepens, the dissipation rates induced by wind forcing and buoyancy loss are mostly comparable. During this period, surface buoyancy loss is dominant, while the peaks in wind-induced dissipation are typically less than those during winter (Figure S6b and S6c).

From December to April, the contribution of wind forcing is greater than that of buoyancy loss, increasing the contribution of wind-driven upper-ocean dissipation to around 70% of the total. As the mixed layer shoals from April onwards, the surface buoyancy flux changes sign, driving less buoyant convection, so that the contribution of wind-driven dissipation increases to around 90%. A strong correlation between the glider-derived

upper-ocean dissipation rate and both time series of buoyancy- and wind-driven dissipation suggests that these simple scalings for the effects of wind- and buoyancy-driven turbulence can explain much of the variation in the observed upper-ocean dissipation. The agreement with the glider-based dissipation rate is particularly strong for the combined buoyancy and wind contributions (R=0.80). These results suggest that upper-ocean dissipation in this area at depths beyond the influence of surface waves, may be characterized by one-dimensional estimates of turbulence induced by air-sea buoyancy fluxes and wind forcing. Further, this comparison demonstrates the changing nature of mixed layer dissipation throughout the year. The wintertime deepening of the mixed layer is driven almost equally by surface buoyancy loss and wind forcing. During the spring however, wind forcing drives the sporadic mixing (and mixed layer deepening) as surface buoyancy gain induces a general shoaling of the mixed layer.

There are short periods when the glider-derived dissipation is elevated and the one-dimensional estimates of turbulence are low, during January, February and March for example. At these times there are several peaks glider dissipation rate that are a factor of two larger than the one-dimensional estimate of turbulence. A comparison with the results of *Thompson et al.* [2016] suggest these periods of disagreement broadly coincide with times at which three-dimensional submesoscale instabilities are more likely. The glider-derived dissipation rate compares well in terms of both magnitude and variability with the ADCP-derived dissipation and matches the variability of estimates from one-dimensional mixed layer scalings. This gives confidence in the validity of our our glider-derived estimate, through a range of stratification levels. Further, these results

suggest that in this region submesoscale instabilities may play a lesser role in driving turbulent dissipation in the upper ocean in contrast to findings in western boundary current environments [*D'Asaro et al.*, 2011].

4. Conclusions

This study documents a full annual cycle of surface to 1000 m turbulent dissipation rate in the ocean, and the physical forcings of its variability. It provides insight into the seasonal variation of the turbulent dissipation in the mid-latitude North Atlantic within the mixed layer, and the relationship between upper-ocean dissipation and the depth of the mixed layer. Further, this analysis highlights the key processes that drive dissipation within the upper ocean and regulate the depth of the ocean surface boundary layer. These results were obtained by generalizing the method to determine turbulent dissipation from standard Seaglider measurements [*Beaird et al.*, 2012] to a wider range of stratification levels. Upper-ocean dissipation is characterized by pulses of elevated turbulence that extend through most of the mixed layer and correspond to periods of a deepening mixed layer. These pulses of dissipation and daily-to-weekly changes in the depth of the mixed layer occur during both winter and spring, as the mixed layer deepens or shoals, respectively.

Here, simple one-dimensional estimates of the mixed layer dissipation driven by air–sea buoyancy and wind forcings capture most of the observed variability of dissipation within the mixed layer deeper than 40 m. This allows a dissection of the relative roles of buoyancy and wind forcings in driving variability in the mixed layer. While buoyancy and wind forcings play a comparable role in the early winter as the mixed layer deep-

ens, wind forcing dominates as a driver of mixed layer dissipation through the rest of the year. This generates, for example, the springtime pulses in dissipation that coincide with short-term deepenings of the mixed layer. Despite missing much of the wave-driven turbulence near the surface, the Seaglider-derived dissipation rate appears to capture the bulk of the variation of upper-ocean turbulence. Short-term deviations between estimates of dissipation rate and the classical forcing-based scalings may be associated with submesoscale processes [*Thompson et al.*, 2016], the effects of which are not represented by the scalings used here. This paper introduces an updated method of determining dissipation rates from standard Seaglider observations, enabling depth-varying estimates of turbulence over many months. Application of this method to existing and future long-duration glider datasets promises further insights into the drivers of turbulent dissipation.

Range Weather Forecasts (downloaded from http://www.ecmwf.int/en/research/climate-reanalysis/era-interim downloaded on the 27 March 2017).

References

Beaird, N., I. Fer, P. Rhines, and C. Eriksen (2012), Dissipation of Turbulent Kinetic Energy Inferred from Seagliders: An Application to the Eastern Nordic Seas Overflows, *Journal of Physical Oceanography*, *42*(12), 2268–2282, doi:10.1175/JPO-D-12-094.1.

Belcher, S. E., A. L. M. Grant, K. E. Hanley, B. Fox-Kemper, L. Van Roekel, P. P. Sullivan, W. G. Large, A. Brown, A. Hines, D. Calvert, A. Rutgersson, H. Pettersson, J.-R. Bidlot, P. A. E. M. Janssen, and J. A. Polton (2012), A global perspective on Langmuir turbulence in the ocean surface boundary layer, *Geophysical Research Letters*, *39*(18), doi:10.1029/2012GL052932.

Bray, N. A., and N. P. Fofonoff (1981), Available Potential Energy for MODE Eddies, *Journal of Physical Oceanography*, *11*(1), 30–47, doi:10.1175/1520-0485(1981)011¡0030:APEFME¿2.0.CO;2.

Buckingham, C. E., A. C. Naveira Garabato, A. F. Thompson, L. Brannigan, A. Lazar, D. P. Marshall, A. J. George Nurser, G. Damerell, K. J. Heywood, and S. E. Belcher (2016), Seasonality of submesoscale flows in the ocean surface boundary layer, *Geophysical Research Letters*, *43*(5), 2118–2126, doi:10.1002/2016GL068009.

Damerell, G. M., K. J. Heywood, A. F. Thompson, U. Binetti, and J. Kaiser (2016), The vertical structure of upper ocean variability at the Porcupine Abyssal Plain during 2012–2013, *Journal of Geophysical Research: Oceans*, *121*(5), 3075–3089, doi:10.1002/2015JC011423.

D'Asaro, E., C. Lee, L. Rainville, L. Thomas, and R. Harcourt (2011), Enhanced Turbulence and Energy Dissipation at Ocean Fronts, *Science*, doi:10.1126/science.1201515.

D'Asaro, E. A. (2014), Turbulence in the Upper-Ocean Mixed Layer, *Annual Review of Marine Science*, *6*(1), 101–115, doi:10.1146/annurev-marine-010213-135138.

D'Asaro, E. A., and R.-C. Lien (2000), Lagrangian Measurements of Waves and Turbulence in Stratified Flows, *Journal of Physical Oceanography*, *30*(3), 641–655, doi: 10.1175/1520-0485(2000)030¡0641:LMOWAT¿2.0.CO;2.

Dee, D. P., S. M. Uppala, A. J. Simmons, P. Berrisford, P. Poli, S. Kobayashi, U. Andrae, M. A. Balmaseda, G. Balsamo, P. Bauer, P. Bechtold, A. C. M. Beljaars, L. van de Berg, J. Bidlot, N. Bormann, C. Delsol, R. Dragani, M. Fuentes, A. J. Geer, L. Haimberger, S. B. Healy, H. Hersbach, E. V. Hólm, L. Isaksen, P. Kållberg, M. Köhler, M. Matricardi, A. P. McNally, B. M. Monge-Sanz, J.-J. Morcrette, B.-K. Park, C. Peubey, P. de Rosnay, C. Tavolato, J.-N. Thépaut, and F. Vitart (2011), The ERA-Interim reanalysis: configuration and performance of the data assimilation system, *Quarterly Journal of the Royal Meteorological Society*, *137*(656), 553–597, doi:10.1002/qj.828.

Dillon, T. M. (1982), Vertical overturns: A comparison of Thorpe and Ozmidov length scales, *Journal of Geophysical Research: Oceans*, *87*(C12), 9601–9613, doi: 10.1029/JC087iC12p09601.

Eriksen, C. C., T. J. Osse, R. D. Light, T. Wen, T. W. Lehman, P. L. Sabin, J. W. Ballard, and A. M. Chiodi (2001), Seaglider: a long-range autonomous underwater vehicle for oceanographic research, *IEEE Journal of Oceanic Engineering*, *26*(4), 424–436, doi: 10.1109/48.972073.

Ferrari, R., and C. Wunsch (2008), Ocean Circulation Kinetic Energy: Reservoirs, Sources, and Sinks, *Annual Review of Fluid Mechanics*, *41*(1), 253–282, doi: 10.1146/annurev.fluid.40.111406.102139.

Ferron, B., H. Mercier, K. Speer, A. Gargett, and K. Polzin (1998), Mixing in the Romanche Fracture Zone, *Journal of Physical Oceanography*, *28*(10), 1929–1945, doi: 10.1175/1520-0485(1998)028¡1929:MITRFZ¿2.0.CO;2.

Frajka-Williams, E., C. C. Eriksen, P. B. Rhines, and R. R. Harcourt (2011), Determining Vertical Water Velocities from Seaglider, *Journal of Atmospheric and Oceanic Technology*, *28*(12), 1641–1656, doi:10.1175/2011JTECHO830.1.

Gargett, A. E. (1989), Ocean Turbulence, *Annual Review of Fluid Mechanics*, *21*(1), 419–451, doi:10.1146/annurev.fl.21.010189.002223.

Gargett, A. E. (1999), Velcro Measurement of Turbulence Kinetic Energy Dissipation Rate ϵ, *Journal of Atmospheric and Oceanic Technology*, *16*(12), 1973–1993, doi: 10.1175/1520-0426(1999)016¡1973:VMOTKE¿2.0.CO;2.

Griffies, S. M., A. Gnanadesikan, K. W. Dixon, J. P. Dunne, R. Gerdes, M. J. Harrison, A. Rosati, J. L. Russell, B. L. Samuels, M. J. Spelman, M. Winton, and R. Zhang (2005), Formulation of an ocean model for global climate simulations, *Ocean Science*, *1*(1), 45–79, doi:10.5194/os-1-45-2005.

Guerra, M., and J. Thomson (2017), Turbulence Measurements From 5-Beam Acoustic Doppler Current Profilers, *Journal of Atmospheric and Oceanic Technology*, (2016), 16–148, doi:10.1175/JTECH-D-16-0148.1.

Horwitz, R. M., and A. E. Hay (2017), Turbulence dissipation rates from horizontal velocity profiles at mid-depth in fast tidal flows, *Renewable Energy*, *114* (August), 283–296, doi:10.1016/j.renene.2017.03.062.

Hoskins, B. (1982), The Mathematical Theory of Frontogenesis, *Annual Review of Fluid Mechanics*, *14*, 131–151, doi:10.1146/annurev.fl.14.010182.001023.

Large, W. G., and S. Pond (1981), Open Ocean Momentum Flux Measurements in Moderate to Strong Winds, *Journal of Physical Oceanography*, *11*(3), 324–336, doi:10.1175/1520-0485(1981)011¡0324:OOMFMI¿2.0.CO;2.

Large, W. G., J. C. McWilliams, and S. C. Doney (1994), Oceanic vertical mixing: A review and a model with a nonlocal boundary layer parameterization, *Reviews of Geophysics*, *32*(4), 363–403, doi:10.1029/94RG01872.

Lhermitte, R. M. (1969), Atmospheric Probing by Doppler Radar.

Li, Q., B. Fox-Kemper, Ø. Breivik, and A. Webb (2017), Statistical models of global Langmuir mixing, *Ocean Modelling*, *113*, 95–114, doi:http://dx.doi.org/10.1016/j.ocemod.2017.03.016.

Liu, H., C.-y. Wu, and J. Ren (2011), Estimation of turbulent kinetic energy dissipation rate in the bottom boundary layer of the Pearl River Estuary, *China Ocean Engineering*, *25*(4), 669–678, doi:10.1007/s13344-011-0053-2.

Lomb, N. R. (1976), Least-squares frequency analysis of unequally spaced data, *Astrophysics and Space Science*, *39*(2), 447–462, doi:10.1007/BF00648343.

Lorke, A. (2007), Boundary mixing in the thermocline of a large lake, *Journal of Geophysical Research*, *112*(C9), C09,019.

Lorke, A., L. Umlauf, and V. Mohrholz (2008), Stratification and mixing on sloping boundaries, *Geophysical Research Letters*, *35*(14), L14,610.

Lucas, N. S., J. H. Simpson, T. P. Rippeth, and C. P. Old (2014), Measuring Turbulent Dissipation Using a Tethered ADCP, *Journal of Atmospheric and Oceanic Technology*, *31*(8), 1826–1837, doi:10.1175/JTECH-D-13-00198.1.

McCaffrey, K., B. Fox-Kemper, P. E. Hamlington, and J. Thomson (2015), Characterization of turbulence anisotropy, coherence, and intermittency at a prospective tidal energy site: Observational data analysis, *Renewable Energy*, *76*, 441–453, doi: 10.1016/j.renene.2014.11.063.

McMillan, J. M., and A. E. Hay (2017), Spectral and Structure Function Estimates of Turbulence Dissipation Rates in a High Flow Tidal Channel Using Broadband ADCPs, *Journal of Atmospheric and Oceanic Technology*, *34*(1).

McMillan, J. M., A. E. Hay, R. G. Lueck, and F. Wolk (2016), Rates of Dissipation of Turbulent Kinetic Energy in a High Reynolds Number Tidal Channel, *Journal of Atmospheric and Oceanic Technology*, *33*(4), 817–837, doi:10.1175/JTECH-D-15-0167.1.

Mohrholz, V., H. Prandke, and H. U. Lass (2008), Estimation of TKE dissipation rates in dense bottom plumes using a Pulse Coherent Acoustic Doppler Profiler (PC-ADP) ? Structure function approach, *Journal of Marine Systems*, *70*(3-4), 217–239, doi: 10.1016/j.jmarsys.2007.03.004.

Moum, J. N. (1996), Energy-containing scales of turbulence in the ocean thermocline, *Journal of Geophysical Research: Oceans*, *101*(C6), 14,095–14,109, doi: 10.1029/96JC00507.

Pollard, R. T., P. B. Rhines, and R. O. R. Y. Thompson (1972), The deepening of the wind-Mixed layer, *Geophysical Fluid Dynamics*, *4*(1), 381–404, doi: 10.1080/03091927208236105.

Polzin, K. L., A. C. Naveira Garabato, T. N. Huussen, B. M. Sloyan, and S. Waterman (2014), Finescale parameterizations of turbulent dissipation, *Journal of Geophysical Research: Oceans*, *119*(2), 1383–1419, doi:10.1002/2013JC008979.

RDInstruments (2011), Acoustic Doppler Current Profiler Principles of Operation A Practical Primer.

Rippeth, T. P., J. H. Simpson, E. Williams, and M. E. Inall (2003), Measurement of the rates of production and dissipation of turbulent kinetic energy in an energetic tidal flow: Red Wharf Bay revisited, *Journal of Physical Oceanography*, *33*(9), 1889–1901.

Rudnick, D. L., and S. T. Cole (2011), On sampling the ocean using underwater gliders, *Journal of Geophysical Research: Oceans*, *116*(C8), n/a—-n/a, doi: 10.1029/2010JC006849.

Rumyantseva, A., N. S. Lucas, T. P. Rippeth, A. P. Martin, S. C. Painter, T. J. Boyd, and S. A. Henson (2015), Ocean nutrient pathways associated with the passage of a storm, *Global Biogeochemical Cycles*, *29*(8), 1179–1189, doi:10.1002/2015GB005097.

Sarmiento, J., and N. Gruber (2006), *Ocean Biogeochemical Dyncamics*, 528 pp., Princeton University Press.

Sauvageot, H. (1992), *Radar Meterology*, 384 pp., Artech House, Norwood, Massachusetts.

Scannell, B. D., J. H. Simpson, J. A. Polton, and J. Hopkins (2017), Correcting surface wave bias in structure function estimates of turbulent kinetic energy dissipation rate.

Shay, T. J., and M. C. Gregg (1984), Turbulence in an oceanic convective mixed layer, *Nature*, *310*, 282 EP –.

Shay, T. J., and M. C. Gregg (1986), Convectively Driven Turbulent Mixing in the Upper Ocean, *Journal of Physical Oceanography*, *16*(11), 1777–1798, doi:10.1175/1520-0485(1986)016¡1777:CDTMIT¿2.0.CO;2.

Sheen, K. L., J. A. Brearley, A. C. Naveira Garabato, D. A. Smeed, S. Waterman, J. R. Ledwell, M. P. Meredith, L. St. Laurent, A. M. Thurnherr, J. M. Toole, and A. J. Watson (2013), Rates and mechanisms of turbulent dissipation and mixing in the Southern Ocean: Results from the Diapycnal and Isopycnal Mixing Experiment in the Southern Ocean (DIMES), *Journal of Geophysical Research: Oceans*, *118*(6), 2774–2792, doi: 10.1002/jgrc.20217.

Simpson, J. H., P. J. Wiles, and B. J. Lincoln (2011), Internal seiche modes and bottom boundary-layer dissipation in a temperate lake from acoustic measurements, *Limnology and Oceanography*, *56*(5), 1893–1906, doi:10.4319/lo.2011.56.5.1893.

Simpson, J. H., N. S. Lucas, B. Powell, and S. C. Maberly (2015), Dissipation and mixing during the onset of stratification in a temperate lake, Windermere, *Liminology and Oceanography*, *60*, 29–41, doi:10.1002/lno.10008.

Talke, S. A., A. R. Horner-Devine, C. C. Chickadel, and A. T. Jessup (2013), Turbulent kinetic energy and coherent structures in a tidal river, *Journal of Geophysical Research: Oceans*, *118*(12), 6965–6981, doi:10.1002/2012JC008103.

Taylor, G. I. (1935), Statistical Theory of Turbulence, *Proceedings of the Royal Society of London A: Mathematical, Physical and Engineering Sciences*, *151*(873), 421–444,

doi:10.1098/rspa.1935.0158.

Tennekes, H., and J. L. Lumley (1972), *A First Course in Turbulence*, {MIT} Press, Cambridge, Massachusetts,.

Thomas, L. N., A. Tandon, and A. Mahadevan (2013), Submesoscale Processes and Dynamics, in *Ocean Modeling in an Eddying Regime*, pp. 17–38, American Geophysical Union, doi:10.1029/177GM04.

Thompson, A. F., A. Lazar, C. Buckingham, A. C. Naveira Garabato, G. M. Damerell, and K. J. Heywood (2016), Open-Ocean Submesoscale Motions: A Full Seasonal Cycle of Mixed Layer Instabilities from Gliders, *Journal of Physical Oceanography*, *46*(4), 1285–1307, doi:10.1175/JPO-D-15-0170.1.

Thomson, J., B. Polagye, M. Richmond, and V. Durgesh (2010), Quantifying turbulence for tidal power applications, *MTS/IEEE Seattle, OCEANS 2010*, (4), doi:10.1109/OCEANS.2010.5664600.

Thomson, J., B. Polagye, V. Durgesh, and M. C. Richmond (2012), Measurements of turbulence at two tidal energy sites in puget sound, WA, *IEEE Journal of Oceanic Engineering*, *37*(3), 363–374, doi:10.1109/JOE.2012.2191656.

Thorpe, S. A. (1977), Turbulence and mixing in a Scottish Loch, *Philosophical Transactions of the Royal Society of London A: Mathematical, Physical and Engineering Sciences*, *286*(1334), 125–181, doi:10.1098/rsta.1977.0112.

Thorpe, S. A. (2005), *The Turbulent Ocean*, Cambridge University Press, doi:10.1017/CBO9780511819933.

Trenberth, K. E., J. G. Olson, and W. G. Large (1990), The mean annual cycle in global ocean wind stress, *Journal of Physical Oceanography*, *20*, 1742–1760.

Watson, A. J., J. R. Ledwell, M.-J. Messias, B. A. King, N. Mackay, M. P. Meredith, B. Mills, and A. C. Naveira Garabato (2013), Rapid cross-density ocean mixing at mid-depths in the Drake Passage measured by tracer release, *Nature*, *501*(7467), 408–411.

Wesson, J. C., and M. C. Gregg (2012), Mixing at Camarinal Sill in the Strait of Gibraltar, *Journal of Geophysical Research: Oceans*, *99*(C5), 9847–9878, doi: doi:10.1029/94JC00256.

Wiles, P. J., T. P. Rippeth, J. H. Simpson, and P. J. Hendricks (2006), A novel technique for measuring the rate of turbulent dissipation in the marine environment, *Geophysical Research Letters*, *33*(21), doi:Artn L21608

Doi 10.1029/2006gl027050.

Wunsch, C., and R. Ferrari (2004), Vertical Mixing, Energy, and the General Circulation of the Oceans, *Ann. Rev. Fluid Mech.*, *36*, 281–314.

Zedel, L., A. E. Hay, R. Cabrera, and A. Lohrmann (1996), Performance of a Single-Beam Pulse-to-Pulse Coherent Doppler Profiler, *Journal of Oceanic Engineering*, *21*(3), 290–297.

Zika, J. D., T. J. McDougall, and B. M. Sloyan (2010), A Tracer-Contour Inverse Method for Estimating Ocean Circulation and Mixing, *Journal of Physical Oceanography*, *40*(1), 26–47, doi:10.1175/2009JPO4208.1.
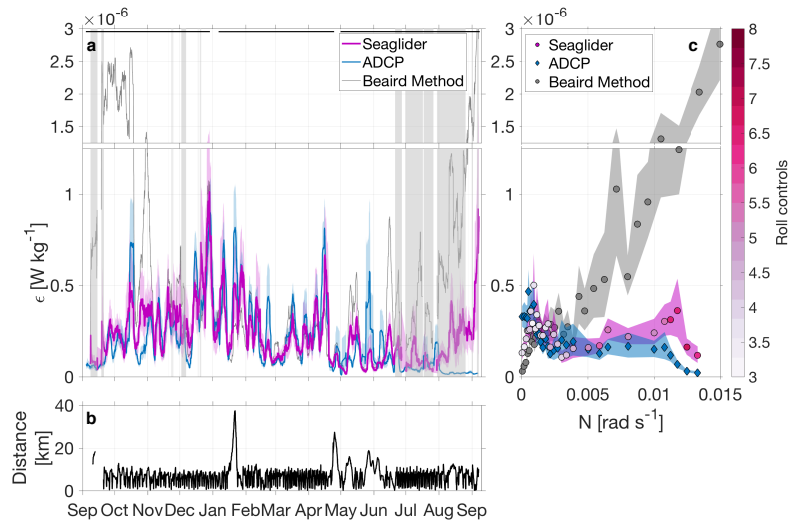
Figure 1. (a) Seaglider-based rate of dissipation (magenta) compared to dissipation rate estimated using the ADCP-based structure function approach (blue) and the original *Beaird et al.* [2012] method to estimate dissipation from glider observations using a fixed 30 m high-pass filter (gray). Time-series are smoothed using a 4-day running mean. The colored shading shows the 90% confidence interval determined using a Monte Carlo approach. The gray shading indicates periods of excessive glider roll maneuvers. An estimate of glider-based dissipation rate is flagged when the number of roll maneuvers in a given 20 m depth bin exceeds 6. The gray shading indicates periods in which more than half the data used to calculate the 4-day average is flagged. The horizontal black bars denote individual glider deployments. (b) Distance between the Seaglider and the ADCP. (c) Seaglider- and ADCP-based dissipation rates averaged into bins of buoyancy frequency, N. Each N-bin contains 100 glider observations. The color of the glider data points indicates the mean number of glider roll maneuvers. The colored shading shows the 90% confidence interval determined using a Monte Carlo approach
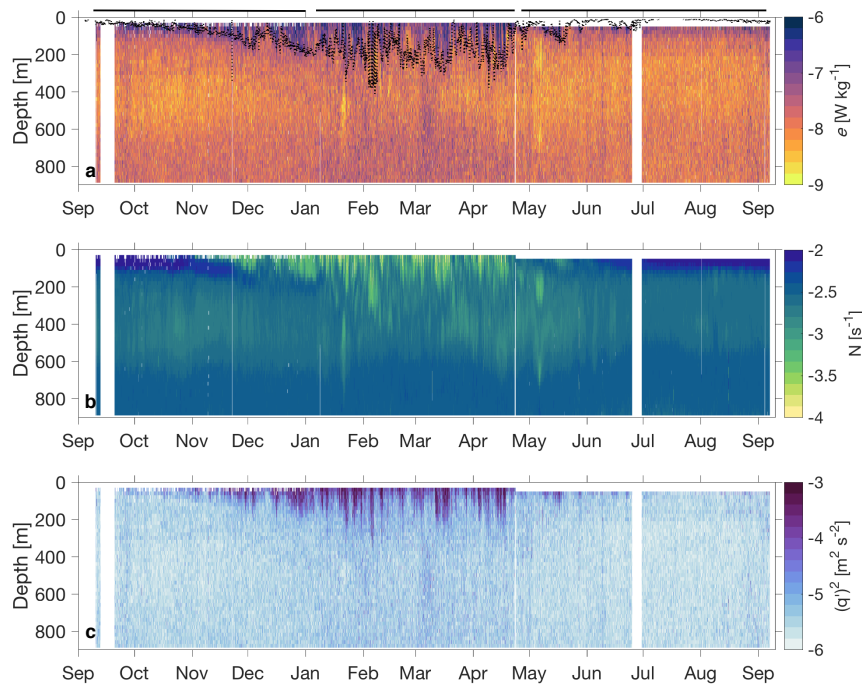
Figure 2. Time series of (a) Seaglider-based dissipation rate e, (b) N and (c) $(q')^2$ from equation (1). Each variable is calculated in 20 m vertical bins from the surface to 900 m. The black line represents the mixed layer depth determined as the depth at which density exceeds the density at 10 m by $0.03\,\mathrm{kg\,m^{-3}}$. The horizontal black bars indicate each individual glider deployment.
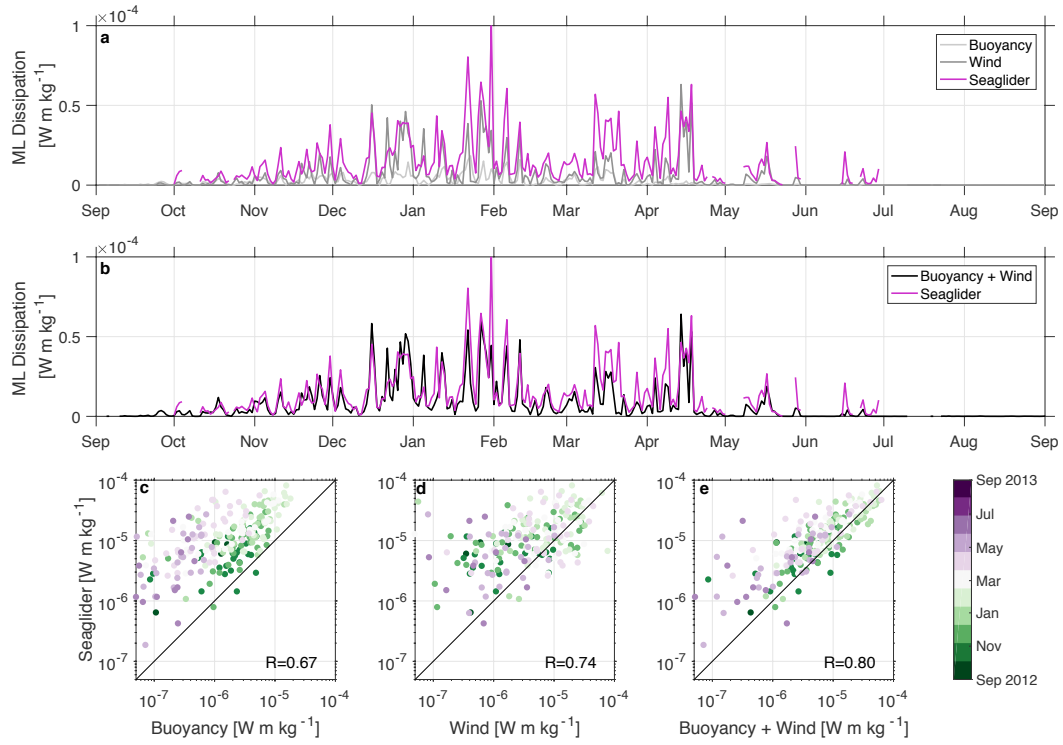
Figure 3. (a) Seaglider-based dissipation rate integrated through the mixed layer (magenta), mixed layer dissipation rate induced by surface buoyancy forcing (light gray; ϵ_Q from equation (3)) and mixed layer dissipation rate induced by surface wind forcing (dark gray; ϵ_τ from equation (4)). (b) Mixed layer glider dissipation rate (magenta) and $\epsilon_Q + \epsilon_\tau$ (black). (c-e) Mixed layer glider dissipation rate plotted against ϵ_Q,ϵ_τ and $\epsilon_Q + \epsilon_\tau$, with colors representing time.